



Spin structure at zero magnetic field and field-induced spin reorientation transitions in a layered organic canted antiferromagnet bordering a superconducting phase

Kohsuke Oinuma, Naoki Okano, Hitoshi Tsunakawa, Shinji Michimura, Takuya Kobayashi , Hiromi Taniguchi ,*
and Kazuhiko Satoh

Graduate School of Science and Engineering, Saitama University, Saitama 338-8570, Japan

Julia Angel and Isao Watanabe


*Meson Science Laboratory, Nishina Center for Accelerator-Based Science, Institute of Physical and Chemical Research (RIKEN),
2-1 Hirosawa, Wako 351-0198, Japan*

Yasuyuki Ishii

Department of Physics, College of Engineering, Shibaura Institute of Technology, Saitama 337-8570, Japan

Hiroyuki Okamoto

Faculty of Medicine, Kanazawa University, Kodatsuno 5-11-89, Kanazawa 920-0942, Japan

Tetsuaki Itou 

Department of Applied Physics, Tokyo University of Science, Tokyo 125-8585, Japan



(Received 21 November 2019; revised 18 June 2020; accepted 19 June 2020; published 1 July 2020)

We attempted to assign the spin structure of a layered organic antiferromagnet, κ -(d8-BEDT-TTF)₂Cu[N(CN)₂]Br, which is a key material located closest to the Mott boundary at ambient pressure among this family of compounds, by investigating its macroscopic magnetization thoroughly, motivated by a recent successful assignment of the spin structure of an isostructural material, κ -(BEDT-TTF)₂Cu[N(CN)₂]Cl [BEDT-TTF and d8-BEDT-TTF are bis(ethylenedithio)tetrathiafulvalene and its deuterated molecule, respectively]. We measured the isothermal magnetization after careful choice of the measurement temperatures and cooling speed at around 80 K, so that the magnetism of the antiferromagnetic phase can be effectively extracted. Consequently, we observed hysteresis loops signifying ferromagnetism and steplike behavior when the magnetic field applied parallel to the crystallographic *b* and *a* axes was swept, respectively. The possible spin structure consistent with these results was discussed in terms of probable interactions between the spins, such as exchange interactions and the Dzyaloshinskii-Moriya interaction. Eventually, we asserted that κ -(d8-BEDT-TTF)₂Cu[N(CN)₂]Br has a spin structure with the easy axis being the *c* axis and the net canted moment parallel to the *b* axis, which is surprisingly different from that of κ -(BEDT-TTF)₂Cu[N(CN)₂]Cl. We suggested that this difference originates from the difference of the sign of the interlayer interaction between the two materials. We also elucidated the overall picture of the magnetization processes of this material under the magnetic fields parallel to the three principle axes, which are also in contrast to those of κ -(BEDT-TTF)₂Cu[N(CN)₂]Cl. In particular, the spin-reverse transition at which half of the spins rotate by 180° was not induced by the *b*-axis magnetic field, as in the case of κ -(BEDT-TTF)₂Cu[N(CN)₂]Cl, but by the *a*-axis magnetic field. Finally, numerical simulations and magnetic symmetry analysis enabled us to confirm the validity of the spin structures proposed for the two antiferromagnets under zero and high magnetic fields.

DOI: [10.1103/PhysRevB.102.035102](https://doi.org/10.1103/PhysRevB.102.035102)

I. INTRODUCTION

Spin structure at zero magnetic field (ZF) is one of the most fundamental properties of magnets. The spin orientation phenomena in such materials can be regarded as a consequence of the collective effect of various interactions acting on the spins. While information on the spin structure

under high magnetic fields is available for selective evaluation of the stronger interaction that is preserved under such conditions, the spin structure at ZF can include information on very weak interactions as well. Therefore, determination of the ZF spin structure may aid the identification of unknown interactions, a deeper understanding of known interactions, and elucidation of the magnetization process under magnetic fields. Recently, we assigned [1] the ZF spin structure of a BEDT-TTF-based antiferromagnet, κ -(BEDT-TTF)₂Cu[N(CN)₂]Cl (h8- κ -Cl), through detailed analyses of

*taniguchi@phy.saitama-u.ac.jp

macroscopic magnetization [BEDT-TTF denotes the organic molecule, bis(ethylenedithio)tetrathiafulvalene]. This assignment brought about such achievements as will be introduced later. Since application of the neutron-diffraction experiment to this class of materials is extremely difficult, this is an important assignment of the ZF spin structure in BEDT-TTF-based magnets.

The crystal structure and molecular arrangement in the molecular layers in $h8\text{-}\kappa\text{-Cl}$ are shown in Figs. 1(a) and 1(b) [2]. Two adjoining layers, referred to as layers A and B, are related by mirror symmetry in the plane formed by anions. In this material, charge carriers are localized at the BEDT-TTF dimers [3], as shown by the blue circles in Fig. 1(b), owing to the Coulomb interaction. Therefore, $h8\text{-}\kappa\text{-Cl}$ is regarded as a Mott insulator [3–7]. This material undergoes antiferromagnetic (AF) ordering at 22.8 K [8]. The interesting features of this spin system are not only the characteristics inherent to BEDT-TTF salts, such as strong two-dimensionality, but also the Dzyaloshinskii-Moriya (DM) interaction [9,10] that originates from the lack of inversion symmetry between the dimers [11] [for example, A1 and A2 in Fig. 1(b)]. Recently, the importance of the spin-orbit interaction and possible DM interaction in such organics have been predicted theoretically [12]. As a consequence of the competition between the DM and intralayer exchange interactions, a canting moment is induced in the antiferromagnetically ordered spins. This is the origin of the weak ferromagnetism observed in earlier studies [3,8,13,14]. In our previous paper [1], we investigated the magnetization of $h8\text{-}\kappa\text{-Cl}$ as functions of the orientation and intensity of the magnetic field. We also performed numerical simulations of the magnetization on the basis of the classical spin model. Through such arguments, we succeeded in assigning the ZF spin structure. Surprisingly, the assigned ZF spin structure was significantly different from that proposed in past studies [3,11]. In this research [1], determination of the direction of the weak ferromagnetism triggered the elucidation of the ZF spin structure. As the DM vector had already been characterized [11,15] in this material, as mentioned later, the spin easy axis could be inferred from the canting direction of the spins. This methodology is also applicable to studies on the ZF spin structure in other κ -type antiferromagnets.

The physical properties of $h8\text{-}\kappa\text{-Cl}$ can be summarized in a pressure-temperature phase diagram, as shown in Fig. 1(c) [16]. This phase diagram is constructed by applying the soft pressure of He gas to this material. Control of the electronic state can also be achieved by substitution of the constituent atom. For example, the material in which Cl is substituted by Br, $\kappa\text{-(BEDT-TTF)}_2\text{Cu[N(CN)}_2\text{]Br}$ ($h8\text{-}\kappa\text{-Br}$), is an ambient-pressure superconductor [17]. Further substitution in this salt results in a unique electronic state. Deuterated $\kappa\text{-Br}$ ($d8\text{-}\kappa\text{-Br}$), where eight hydrogens in the ethylene groups of BEDT-TTF are substituted by deuteriums, is considered to be located in the vicinity of the superconductor-insulator boundary [18–23], as shown in Fig. 1(c). This close proximity to the boundary is suggested by the fact that this material has very low critical pressure [24] for the insulator-superconductor transition. This is also evidenced by the peculiar physical properties of $d8\text{-}\kappa\text{-Br}$: a single crystal includes a major fraction of the AF insulating (AFI) phase and a minor fraction of the superconducting (SC) phase [18,25–27], similar to $\kappa\text{-Cl}$

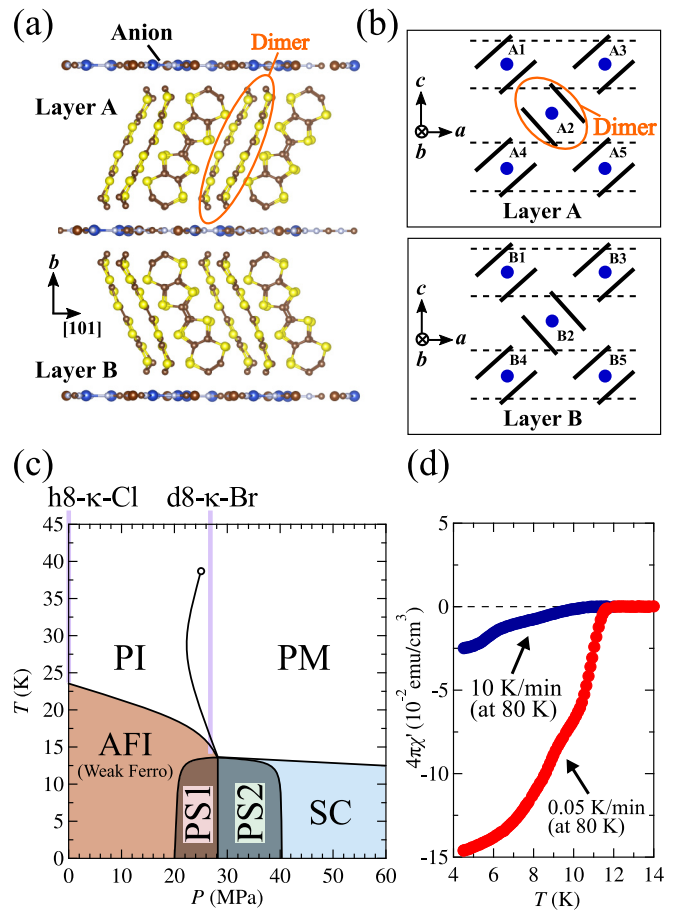


FIG. 1. (a) Crystal structure of $d8\text{-}\kappa\text{-Br}$ and $h8\text{-}\kappa\text{-Cl}$. The orange ellipse stands for the dimer of BEDT-TTF. All the atoms forming each anion layer are located in a single plane, which plays a role of a mirror plane. We refer to two molecular layers related by mirror symmetry with respect to the anion plane as layers A and B. (b) Schematic molecular structure within layers A and B. Blue solid circles denote the localized electrons and the positions of the magnetic sublattice referred to as A1–B5. Dashed lines denote the glide symmetry in the ab plane. (c) Phase diagram of $h8\text{-}\kappa\text{-Cl}$, which consists of paramagnetic insulating (PI), metallic (M), antiferromagnetic insulating (AFI), and superconducting (SC) phases. PS1 and PS2 represent the phase separation between AFI and SC phases: PS1 is the AFI phase with a minor SC phase, and PS2 is the SC phase with a minor AFI phase. Vertical lines at 0 and 27 MPa represent the location of (ambient pressure) $h8\text{-}\kappa\text{-Cl}$ and (ambient pressure) $d8\text{-}\kappa\text{-Br}$, respectively. (d) Temperature dependence of ac susceptibility of $d8\text{-}\kappa\text{-Br}$ after slow cooling (0.05 K/min) and rapid cooling (10 K/min) at around 80 K. The ac field applied parallel to the crystallographic b axis is 0.2 Oe in amplitude and 3.1 Hz in frequency in both the measurements.

at pressures in the range 20 to 28 MPa. This is understood as a phase-separation phenomenon [28–31] near the first-order transition. The volume fraction of this SC phase is at most 15% in our samples, which depends on the cooling speed at around 80 K [18,26,32], as observed in Fig. 1(d). This cooling rate dependence has been interpreted as the disorder effect that originates from the structural glass transition in ethylene groups of BEDT-TTF, at around 80 K [33–35].

In this manner, the d8- κ -Br salt is a key material located closest to the AFI-SC boundary at ambient pressure among this family of compounds. This material is a precious ambient-pressure antiferromagnet, and its magnetism has been investigated by dc susceptibility and ^1H - and ^{13}C -NMR measurements [18,25] under magnetic fields as well as by ZF muon spin rotation (μSR) measurements [36]. The results of those studies have allowed us to conclude that h8- κ -Cl and d8- κ -Br have different magnetic parameters such as localized moment and Néel temperature T_N , but possess common spin structure. For example, ^{13}C -NMR studies [11,15] suggested that the spin structure of d8- κ -Br under high magnetic fields parallel to the crystallographic a axis is the same as that of h8- κ -Cl. However, the ZF spin structure of d8- κ -Br is still unknown. The methodology we applied to h8- κ -Cl may solve this problem in d8- κ -Br as well.

In this paper, we performed isothermal magnetization measurements of d8- κ -Br as functions of the orientation and intensity of the magnetic fields. The contribution of the minor SC phase is a significant problem when analyzing the “magnetism” of this material. To eliminate or suppress this contribution as much as possible, we carefully selected the measurement temperature and cooling speed at around 80 K before conducting magnetization measurements. Consequently, we successfully determined the direction of the weak ferromagnetism and elucidated the magnetization behavior of the AFI phase in various field orientations. The results enabled us to conclude that the ZF spin structure of d8- κ -Br is different from that of h8- κ -Cl. The difference in the pattern of field-induced spin reorientations between the two materials is also suggested and fully understood by using our model. The claimed ZF spin structure and field-induced spin reorientations were supported by the results of numerical simulations and magnetic symmetry analysis.

II. EXPERIMENTAL PROCEDURE

Single crystals of d8- κ -Br were synthesized electrochemically [37,38] on platinum electrodes at a constant current of $0.5 \mu\text{A}$, by employing deuterated BEDT-TTF, $\text{Ph}_4\text{PN}(\text{CN})_2$, and CuBr (Aldrich 99.999%), in a 95% volume of 1,1,2-trichloroethane and 5% volume of ethanol. In our deuterated BEDT-TTF molecule, more than 99% of the hydrogens were enriched by deuteriums. For the electrochemical synthesis, we also referred to reported methods for [39] the synthesis of high-quality crystals of h8- κ -Br. The reaction was carried out at 30°C and the crystals were harvested after 40 days. The obtained crystals were thick and had the shape of distorted hexagons.

Several of the largest single crystals, the weights of which ranged from 7.86 to 21.31 mg, were selected from different batches [38]. These large crystals facilitate the collection of high signal-to-noise ratio data for susceptibility and magnetization. The crystallinity and crystallographic orientation were examined from Laue x-ray photographs. By analyzing the Laue data, we confirmed that our samples were single crystals and identified the crystallographic axes.

The ac susceptibility and magnetization measurements were performed using a superconducting quantum interference device magnetometer (Quantum Design MPMS XL-7).

We used one piece of a single crystal for all measurements. The ac susceptibility was measured as a function of temperature under a zero dc field with an ac field of 0.2 Oe in amplitude and 3.1 Hz in frequency. The ac field was applied parallel to the b axis. Isothermal magnetization was measured as a function of applied magnetic field in various field orientations. The magnetic field was applied nearly parallel to the crystallographic a , b , and c axes as well as several directions in the ac plane. Details of the procedure for the field-orientation dependence of the magnetization were given in our previous paper [1].

Because the cooling speed at approximately 80 K was known to affect the low-temperature electronic state of d8- κ -Br [18,22,26,32], the sample was cooled to 4.5 K with fixed cooling speeds before the measurements. The cooling speeds examined in this paper were 0.05, 0.1, 0.4, and 10 K/min. We selected the appropriate cooling speed depending on the purpose of the measurement. This selection was crucial to effectively extract information of the magnetism of this material, as described later.

III. RESULTS

A. Magnetization under a magnetic field parallel to the ac plane

In our previous paper [1], the direction of the weak ferromagnetism was a key issue in solving the ZF spin structure of h8- κ -Cl, as mentioned above. We investigated the magnetization (M) of h8- κ -Cl at fixed temperatures as a function of applied magnetic field (H) in various field orientations. A series of the results is shown in Fig. 2(b). In the measurements, we changed the field orientation in a stepwise manner within the ac plane, in which the field orientation was defined by θ , the azimuthal angle from the c axis. As observed in Fig. 2(b), the M - H curve exhibits systematic variation, depending on θ .

Figure 2(a) displays the results of d8- κ -Br in the field configuration, similar to that in Fig. 2(b). All the data sets are plotted after subtracting the core's contribution of -4.7×10^{-4} emu/mol [18] (all the data presented hereafter are plotted after the same treatment). As observed in Fig. 2(a), the behavior differs significantly from that of h8- κ -Cl. The residual magnetization is clearly observed in the numerous M - H curves of h8- κ -Cl, whereas all the M - H curves of d8- κ -Br appear to cross the origin, except for the data in the range of -1 – 1 kOe. The small hysteresis behaviors near ZF likely originate from the pinned vortices of superconductivity, which are caused by slight misalignment or tiny crystals grown on the surface of the main crystal. Thus, we estimated the residual magnetizations for the two materials by fitting the data linearly except for the hysteresis region: the data in the ranges of 1 – 2 and -2 – -1 kOe were used in d8- κ -Br and those in the ranges of 0.5 – 2 and -2 – -0.5 kOe were used in h8- κ -Cl (also, in h8- κ -Cl, a tiny superconducting phase may be induced by the thermal contraction of grease used for fixing the sample). Figure 3 depicts the results of fitting, which are plotted as a function of θ . The periodic data of h8- κ -Cl with a maximum at around $\theta = 90^\circ$ clearly indicate that weak ferromagnetism is produced parallel to the a axis. On the other hand, no residual magnetization was observed in d8- κ -Br, suggesting that d8-

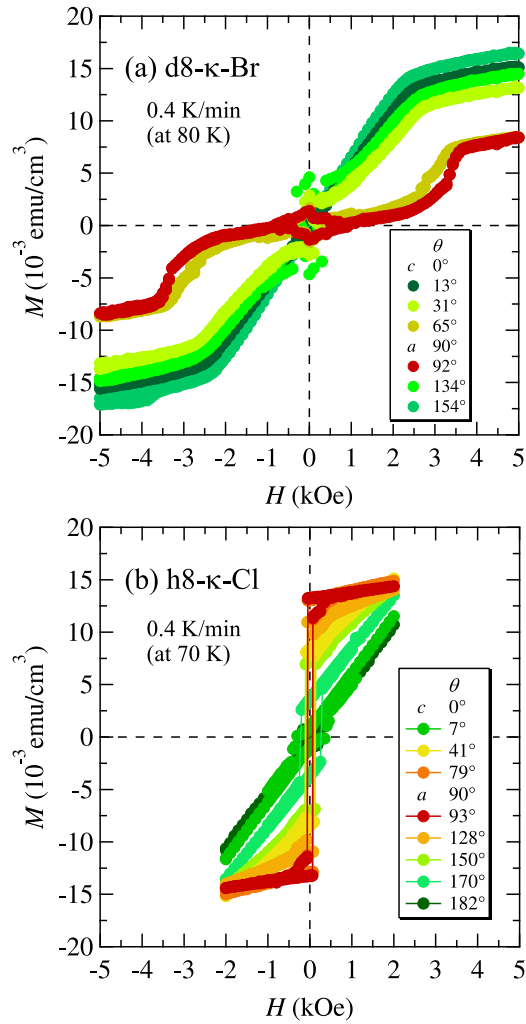


FIG. 2. Magnetic-field (H) dependences of magnetization (M) of d8- κ -Br at 5.5 K (a) and h8- κ -Cl at 5.0 K (b) for various field orientations within the ac plane. θ is the azimuthal angle from c to a . The core's contribution of -4.7×10^{-4} emu/mol [18] has already been subtracted for both materials.

κ -Br is not a weak ferromagnet or that weak ferromagnetism does not exist in the ac plane. In this manner, it is revealed that the ZF spin structure of d8- κ -Br, surprisingly, differs from that of h8- κ -Cl.

While the magnetization in low-field conditions, for example, 1.5 kOe, of h8- κ -Cl increases with the field orientation approaching the a axis, the behavior of d8- κ -Br is contrary to that. In addition, the data with $\theta = 65^\circ$ and 92° exhibit steplike behaviors at approximately 3.5 kOe. These field directions are nearly parallel to the a axis, which is the axis in which h8- κ -Cl exhibits the weak ferromagnetism. These contrasting behaviors between the two materials will be crucial for determining the ZF spin structure of d8- κ -Br.

It should be noted that we have already reported the M - H measurements of d8- κ -Br in the parallel field configuration [36]. We previously examined two types of field orientations and observed almost no difference between them. Unfortunately, we selected the field direction nearly parallel to the $[1\ 0\ 1]$ ($\theta = 45^\circ$) and $[1\ 0\ -1]$ ($\theta = 135^\circ$) directions and could

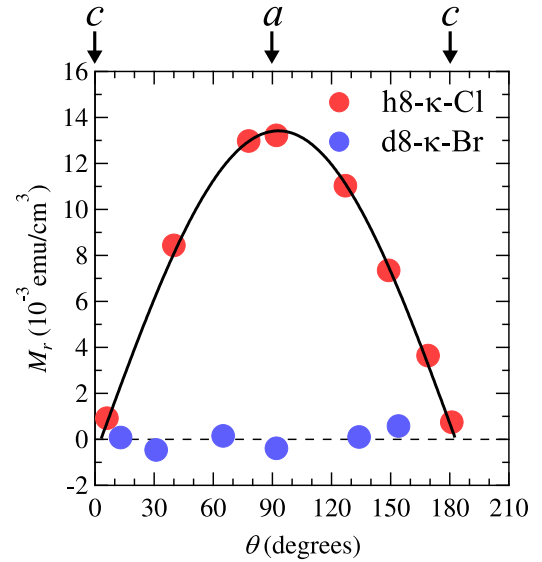


FIG. 3. Residual magnetizations of d8- κ -Br and h8- κ -Cl as a function of θ . The values of θ corresponding to crystallographic axes, a and c , are shown. The solid line is a fitting line with $M_r(\theta) = M_{r0} \sin(\theta + \alpha)$ with constants M_{r0} and α .

not confirm the existence of an in-plane anisotropy in the M - H curve. However, our previous data agree well with the present data at approximately $\theta = 45^\circ$ and 135° .

B. Magnetization under magnetic field parallel to the b axis

The experiments mentioned above clearly reveal that the direction of the weak ferromagnetism of d8- κ -Br is missing in the ac plane, contrary to expectations. Therefore the measurement along the other axis, i.e., the b axis, becomes increasingly important. However, as mentioned previously, the existence of the phase-separated SC phase makes it difficult to extract the information of the magnetism of the AFI phase from the measurements in this perpendicular field configuration. It will become more difficult at lower temperatures, owing to the growth of the superconductivity. Accordingly, we focus on the physical properties of d8- κ -Br at higher temperatures, i.e., the properties near T_N . The phase diagram in Fig. 1(c) contains a narrow but finite temperature range in which $T_c^m < T < T_N$ holds, where T_c^m is defined as a transition temperature of the minor SC phase. In this temperature range, we can evaluate the magnetism of the pure AFI phase or the AFI phase with slight paramagnetic impurity. Next, we introduce another important fact regarding the magnetism of this material. We performed ZF- μ SR measurements on d8- κ -Br cooled at slow [36] and fast cooling speeds [40]. The μ SR spectrum of d8- κ -Br just below T_N was found to change by the effect of the fast cooling whereas the low-temperature spectra were almost unchanged. The disorder induced by the fast cooling affects not only the minor SC phase, as observed in Fig. 1(d), but also the AFI phase near T_N . Therefore, to measure the intrinsic magnetism near T_N , we must cool the sample slowly.

Figure 4 presents the results of the M - H measurements in the perpendicular field configuration ($H \parallel b$) for various temperatures. Hereafter, the magnetic fields parallel to the

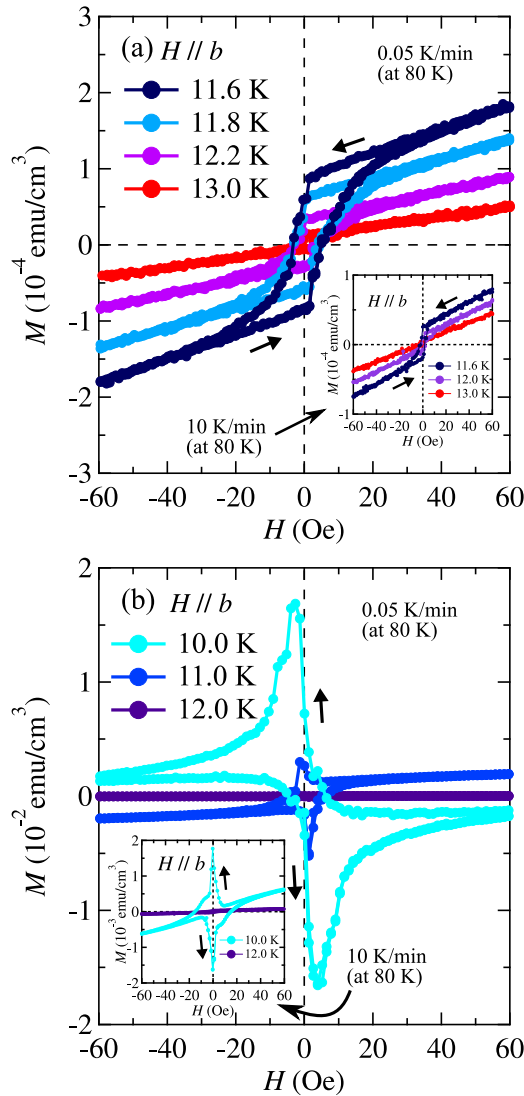


FIG. 4. M - H curves of $d8\text{-}\kappa\text{-Br}$. The magnetic field applied parallel to the b axis was swept in field-ascending and field-descending processes. Because the curves of raw data were not centrosymmetric, owing to residual magnetic fields, we shifted all the data by approximately 3 Oe. (a) M - H curves obtained at 11.6, 11.8, 12.2, and 13.0 K after slow cooling (0.05 K/min) at approximately 80 K. Inset: Data obtained at 11.6, 12.0, and 13.0 K after rapid cooling (10 K/min). (b) Data obtained at 10.0, 11.0, and 12.0 K after slow cooling at approximately 80 K. Inset: Data obtained at 10.0 and 12.0 K after rapid cooling.

a , b , and c axes are referred to as H_a , H_b , and H_c , respectively. First, according to the above discussion, we examined the measurements under H_b after very slow cooling (0.05 K/min). As observed in Fig. 4(a), the data of 11.6, 11.8, and 12.2 K clearly exhibit the residual magnetizations and so-called hysteresis loops. The appearance of the hysteresis loop near T_N and its growth with temperatures lowered suggest that the antiferromagnetism of $d8\text{-}\kappa\text{-Br}$ accompanies the weak ferromagnetism, similar to that of $h8\text{-}\kappa\text{-Cl}$, where T_N is 11.8 K [36] in the moderately slow cooling condition (0.4 K/min) and is slightly higher than 11.8 K in the present condition. In the case of the fast cooling (10 K/min), this

behavior is suppressed but is still visible, as observed in the inset. This cooling rate dependence strongly suggests that such a ferromagnetic behavior does not originate from extrinsic effects such as magnetic impurities but from $d8\text{-}\kappa\text{-Br}$ itself. Thus, the spontaneous magnetization of $d8\text{-}\kappa\text{-Br}$ was observed for the first time. With decreasing temperature, a huge peak appears at around ZF, as observed in Fig. 4(b). This behavior is similar to that of $h8\text{-}\kappa\text{-Br}$ [41–44] and is due to the pinned vortices of superconductivity, as mentioned above. In this manner, the behavior of the spontaneous magnetization is observable only in the narrow temperature range ($\sim 11.5 < T < \sim 12.2$ K). The very slow cooling treatment is also required to clearly observe this behavior. These restrictions are a reason for why the spontaneous magnetization of $d8\text{-}\kappa\text{-Br}$ has not been observed until now. As described in the previous section, the weak ferromagnetism does not have a - and c -axis components. Hence, we conclude that the direction of the net canting moment of $d8\text{-}\kappa\text{-Br}$ is just the b axis, which contrasts the weak ferromagnetism parallel to the a axis in $h8\text{-}\kappa\text{-Cl}$.

C. Cooling rate dependence of magnetization under a magnetic field up to 70 kOe parallel to the b axis

As another strategy for studying the AFI phase of $d8\text{-}\kappa\text{-Br}$, the magnetization measurement at temperatures far lower than T_N after rapid cooling is worth examining. This is because the superconductivity of the minor SC phase can be effectively suppressed, but the magnetism of the AFI phase is almost unchanged in such a condition, as indicated by the μ SR measurements mentioned above. First, we attempted the magnetization measurement under H_b at 2.0 K after the sample was cooled rapidly. In this case, however, the influence of the minor SC phase is still too strong, so the magnetization of the AFI phase in a large part of the low-field region is masked by the diamagnetism and the central peak in the field-ascending and field-descending processes, respectively. Then, we conducted M - H measurements under H_b at a slightly elevated temperature. Figure 5 depicts the obtained M - H curves for various cooling speeds. Data were always obtained in the field-descending process from 70 kOe to 0 Oe at 4.5 K. As observed in the inset, the M - H curve in the low-field region exhibits an appreciable cooling-rate dependence, which must be caused by the variation in the volume fraction of the superconductivity. On the other hand, the magnetizations under H_b that exceed a few dozen kOe do not depend on the cooling rate, as observed in the figure. Hence, the rapid-cooled $d8\text{-}\kappa\text{-Br}$ under such high fields can be regarded as a mixture of the AFI phase and a minor fraction of the paramagnetic one, which would be varied from the SC phase by the magnetic field and/or disorder effect. Because the magnitude of the magnetization of such a paramagnetic phase would be negligible compared to that of the AFI phase, we should only be worried about underestimating the magnetization of the AFI phase. If we adopt the volume fraction of the SC phase in the slowest cooling rate [Fig. 1(c)] as that of the minor phase, the degree of underestimation is approximately 15%.

In addition to the observation mentioned above, the data of 10 K/min seem to maintain their linear trend until ZF, except for a small upward change below 5 kOe due to the pinned

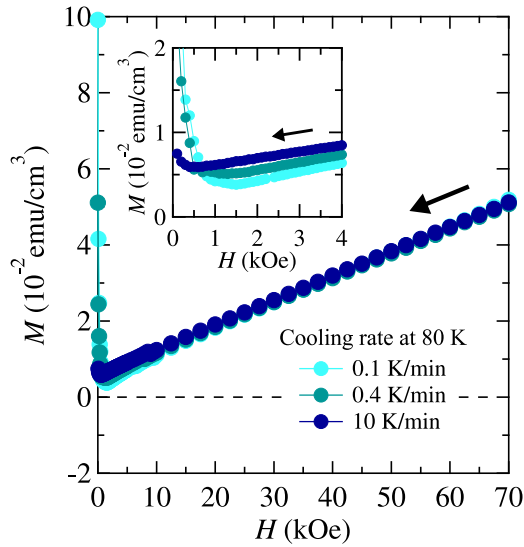


FIG. 5. Cooling-rate dependence of the isothermal magnetization curve of d8- κ -Br at 4.5 K. The magnetic field was applied parallel to the b axis. Data are taken via the field-descending process from 70 kOe after the sample was cooled at different cooling speeds (0.1, 0.4, and 10 K/min) at approximately 80 K.

vortices in the residual SC phase. Discussions in the following section will enable us to suggest that the linear dependence until “ZF” is intrinsic for this perpendicular magnetization. In this sense, the entire data of 10 K/min above 0.5 kOe may be regarded as the magnetization of the pure AFI phase at the qualitative level. Furthermore, because the influence of the minor SC phase is the strongest in this perpendicular configuration, the magnetization measured under H_a and H_c that is at least larger than 0.5 kOe can also be regarded as the magnetization of the AFI phase. For those reasons, we will qualitatively discuss all the magnetizations measured after rapid cooling under magnetic fields above 0.5 kOe and quantitatively evaluate ones under magnetic fields above 30 kOe. The qualitative and quantitative discussions will be conducted in the next section and Sec. IV D, respectively.

D. Magnetizations under magnetic field up to 70 kOe parallel to crystallographic axes

Figure 6(a) presents the isothermal magnetization as functions of magnetic fields parallel to the three crystallographic axes. The data were taken at 4.5 K after the sample was cooled rapidly (10 K/min). This temperature is insufficiently low to be considered as the temperature where the magnetization has reached nearly its maximum in d8- κ -Br, but it is lower than $T_N/2$ (11.8 K) under moderately slow cooling conditions (0.4 K/min).

As observed in Fig. 6(a), the M - H curves for the three axes exhibit contrasting behaviors. Hereafter, the magnetizations under H_a , H_b , and H_c are referred to as $M(H_a)$, $M(H_b)$, and $M(H_c)$, respectively. In $M(H_a)$, a steplike behavior is observed at approximately 3.5 kOe. Because the field orientation is parallel to the conducting plane in this case, the superconductivity of the minor SC phase has almost no influence on this behavior appearing above 0.5 kOe, as explained above.

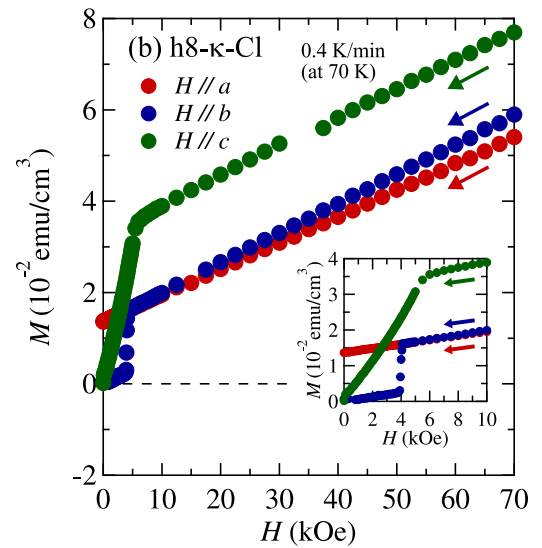
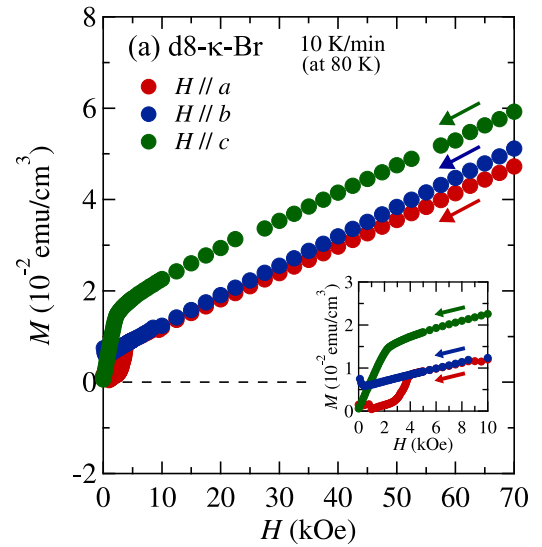


FIG. 6. Isothermal magnetizations of d8- κ -Br at 4.5 K (a) and h8- κ -Cl at 5.0 K (b) as functions of magnetic fields parallel to the three crystallographic axes. Data are taken in field-descending processes from 70 kOe after the samples of d8- κ -Br and h8- κ -Cl are cooled at 10 and 0.4 K/min, respectively. Insets: Magnetization processes under magnetic field lower than 10 kOe.

Furthermore, because this behavior well reproduces the data at $\theta \sim 90^\circ$ in Fig. 2(a), which are obtained at a different cooling speed, it is evident that this steplike behavior is inherent for the AFI phase. The $M(H_c)$ data exhibit a steeper variation under a low field, a change in slope at approximately 2 kOe, and gradual variation under a high field. Because the influence of the superconductivity is suppressed in this case, it is almost certain that this behavior originates from the nature of the AFI phase.

Figure 6(b) shows the corresponding results of h8- κ -Cl for comparison. Although the magnitude of the magnetization of h8- κ -Cl is larger than that of d8- κ -Br in almost the entire field region, the overall shapes of the M - H curves for the three axes are roughly similar to each other. In particular, $M(H_c)$ for the two materials share a characteristic profile, except for the different values of the field at which a kink structure

appears (≈ 2 kOe for d8- κ -Br and ≈ 5 kOe for h8- κ -Cl). On the other hand, $M(H_a)$ and $M(H_b)$ in the low-field region differ between the two materials, as observed in the insets of Figs. 6(a) and 6(b). Interestingly, when the b -axis behavior of d8- κ -Br below 0.5 kOe, which has been modified by the pinned vortices of the minor SC phase, is neglected, two M - H profiles seem to be exchanged by each other: $M(H_a)$ of d8- κ -Br is similar to $M(H_b)$ of h8- κ -Cl, and $M(H_b)$ of d8- κ -Br is similar to $M(H_a)$ of h8- κ -Cl. We observed clear spontaneous magnetization under the b -axis magnetic field near T_N in d8- κ -Br, as mentioned in Sec. III B, and the AFI phase in the present condition is highly expected to exhibit such a behavior. Accordingly, if there was no minor SC phase, $M(H_b)$ of d8- κ -Br would probably exhibit a linear dependence until ZF, similar to $M(H_a)$ of h8- κ -Cl. The AFI phase of d8- κ -Br is known to be disordered compared to that of h8- κ -Cl, owing to the structural glass transition. The gradual steplike behavior in $M(H_a)$ of d8- κ -Br at ≈ 3.5 kOe is affected by this disorder. In this sense, if the disorder did not exist, $M(H_a)$ of d8- κ -Br may exhibit a sharp magnetization jump, similar to $M(H_b)$ of h8- κ -Cl. In this manner, it is more likely for the behaviors of $M(H_a)$ and $M(H_b)$ in h8- κ -Cl to be replaced by the reverse combination in d8- κ -Br. This reversal phenomenon of the two M - H profiles is a very important clue for determining the ZF spin structure of d8- κ -Br.

IV. DISCUSSIONS

A. DM vectors of d8- κ -Br

In the crystal structure of h8- κ -Cl shown in Figs. 1(a) and 1(b), two DM vectors, \mathbf{D}_A and \mathbf{D}_B , are defined for layers A and B, respectively [11]. According to the symmetry analysis conducted by Smith *et al.*, these two vectors can be written as $\mathbf{D}_A = (-D_a, D_b, 0)$ and $\mathbf{D}_B = (D_a, D_b, 0)$, with positive components D_a and D_b [11]. Furthermore, Smith *et al.* performed ^{13}C -NMR measurements on h8- κ -Cl while changing the orientation of an external field [15]. This experiment enables us to determine the directions of the DM vectors precisely and conclude that $D_a \simeq D_b$. Thus, the DM vectors of h8- κ -Cl are inclined by $\pm 45^\circ$ to the b axis. The isostructural d8- κ -Br should also have DM vectors $\mathbf{D}_A = (-D_a, D_b, 0)$ and $\mathbf{D}_B = (D_a, D_b, 0)$. In this material, although it is not proved whether $D_a \simeq D_b$ holds, the orientations of the DM vectors of d8- κ -Br do not differ largely from those of the isostructural h8- κ -Cl. In the following section, we discuss the magnetic properties of d8- κ -Br, assuming this relation for simplicity.

B. Reasoning for zero-field spin structures of d8- κ -Br

In our previous paper [1], we discussed the mechanism for constructing the ZF spin structure of h8- κ -Cl by modeling its spin system. h8- κ -Cl salt and d8- κ -Br salt are considered to possess at least an intralayer AF interaction and an intralayer DM interaction. The energy expressions of the former, E_{AF} , and the latter, E_{DM} , are

$$E_{AF} = 2A_{\parallel}(\mathbf{M}_{A1} \cdot \mathbf{M}_{A2} + \mathbf{M}_{B1} \cdot \mathbf{M}_{B2}), \quad (1)$$

$$E_{DM} = \mathbf{D}_A \cdot (\mathbf{M}_{A1} \times \mathbf{M}_{A2}) + \mathbf{D}_B \cdot (\mathbf{M}_{B1} \times \mathbf{M}_{B2}), \quad (2)$$

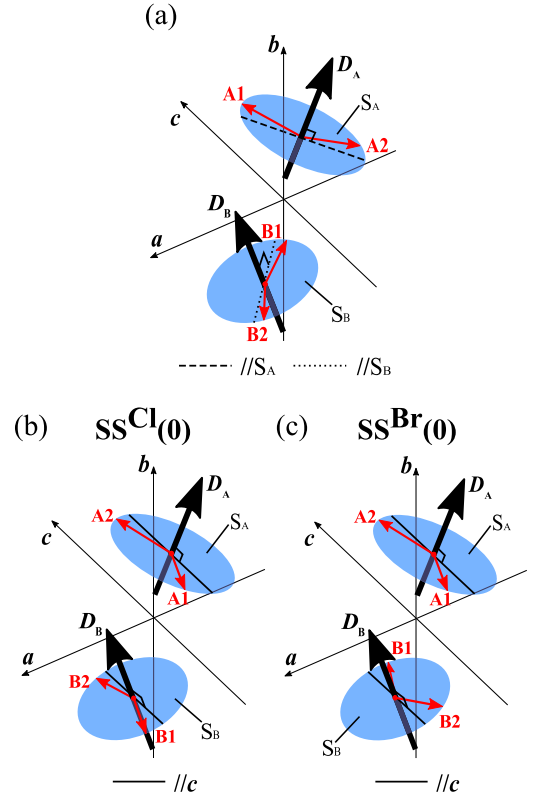


FIG. 7. (a) Possible spin structure in the presence of the intralayer AF interaction and the DM interaction, where red and black arrows denote local moments at the A1–B2 sublattices and DM vectors in layers A and B defined as \mathbf{D}_A and \mathbf{D}_B , respectively. The canting angles of the local moments are exaggerated. S_A and S_B are the planes perpendicular to \mathbf{D}_A and \mathbf{D}_B , respectively. In this case, local moments can lie within S_A (S_B) for layer A (B). (b) Spin structure proposed for h8- κ -Cl at ZF, $SS^{Cl}(0)$, in the presence of interlayer FM interaction in addition to the interactions in the case of (a). (c) Spin structure proposed for d8- κ -Br at ZF, $SS^{Br}(0)$, in the presence of interlayer AF interaction in addition to the interactions in the case of (a).

where A_{\parallel} and $\mathbf{M}_{A1} - \mathbf{M}_{B2}$ are the intralayer isotropic exchange parameter and sublattice magnetization, respectively. If these two interactions are considered, the possibility of the spin orientation in layer A is restricted to a certain extent, as demonstrated in Fig. 7(a). The local moments at the A1 and A2 sites, \mathbf{m}_{A1} and \mathbf{m}_{A2} (red arrows in the figure), respectively, are roughly antiparallel to each other, owing to the strong AF interaction and relatively weak DM interaction. In addition, the vector, $\mathbf{m}_{A1} \times \mathbf{m}_{A2}$, is strictly antiparallel to the DM vector, \mathbf{D}_A , under the condition that the local DM energy, $\mathbf{D}_A \cdot (\mathbf{m}_{A1} \times \mathbf{m}_{A2})$, should be minimized. Accordingly, the roughly antiparallel pair, \mathbf{m}_{A1} and \mathbf{m}_{A2} , appear to have freedom of rotation within the plane, S_A (the blue disk in the figure), which is defined as the plane perpendicular to \mathbf{D}_A . A similar situation is realized in layer B, in which \mathbf{m}_{B1} and \mathbf{m}_{B2} are the local moments at the B1 and B2 sites, respectively, and S_B is the plane perpendicular to the DM vector, \mathbf{D}_B .

Next, we apply interlayer interaction to this virtual spin system. When interlayer ferromagnetic interaction is added to this situation, regardless of how weak it is, all the spin

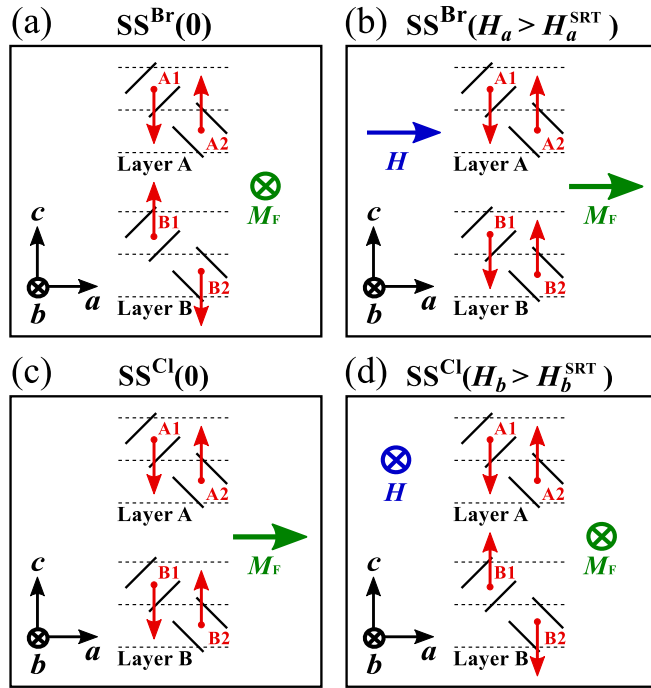


FIG. 8. (a) ZF spin structure proposed for d8- κ -Br, $SS^{\text{Br}}(0)$. (b) Proposed spin structure of d8- κ -Br under H_a ($> H_a^{\text{SRT}}$), which is referred to as $SS^{\text{Br}}(H_a > H_a^{\text{SRT}})$. (c) ZF spin structure proposed for h8- κ -Cl, $SS^{\text{Cl}}(0)$. (d) Proposed spin structure of h8- κ -Cl under H_b ($> H_b^{\text{SRT}}$), which is referred to as $SS^{\text{Cl}}(H_b > H_b^{\text{SRT}})$.

orientations are uniquely fixed, as demonstrated in Fig. 7(b). In this case, all the local moments (or spins) appear to be roughly parallel to the c axis, and the net canting moment appears to be directed towards the a axis. Thus, the constructed spin structure is just the ZF spin structure of h8- κ -Cl, with the spin easy axis being the c axis and the weak ferromagnetism parallel to the a axis, as described in our previous paper [1]. In this paper, the spin structure of h8- κ -Cl at ZF is referred to as $SS^{\text{Cl}}(0)$ and is also depicted in Figs. 8(c) and 9(c) with different expression methods. On the other hand, when interlayer antiferromagnetic interaction acts on this system, the spin structure shown in Fig. 7(c) appears to be constructed. In this case, all the spins are roughly parallel to the c axis but, unlike the above case, the net canting moment is parallel to the b axis. This direction of the net canting moment coincides with the observed direction of the weak ferromagnetism in d8- κ -Br. This spin structure, referred to as $SS^{\text{Br}}(0)$, is also shown in Figs. 8(a) and 9(a).

In this manner, the ZF spin structures of the two materials could be understood from this simple model, in which three types of interactions are considered. Summarizing the above findings, the examination in this model enables us to suggest that the difference between the ZF spin structures of the two materials is caused only by the difference in the “sign” of the interlayer interaction. The spin structure predicted for d8- κ -Br, $SS^{\text{Br}}(0)$, has the easy axis as the c axis, the net canting moment parallel to the b axis, and the antiferromagnetic spin formation in the interlayer direction. In the following section, we will discuss the magnetic properties under high magnetic

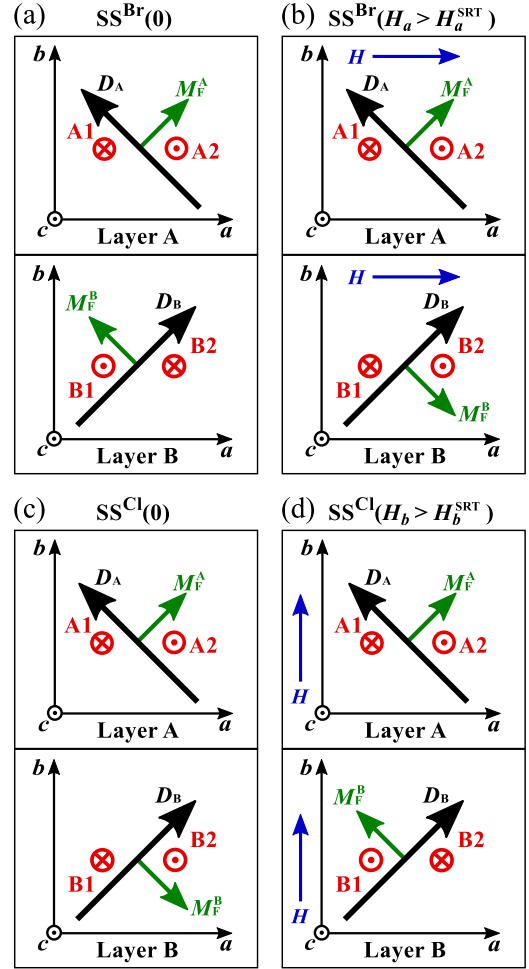


FIG. 9. (a) ZF spin structure of d8- κ -Br, $SS^{\text{Br}}(0)$. (b) Spin structure of d8- κ -Br under H_a ($> H_a^{\text{SRT}}$), $SS^{\text{Br}}(H_a > H_a^{\text{SRT}})$. (c) ZF spin structure of h8- κ -Cl, $SS^{\text{Cl}}(0)$. (d) Spin structure of h8- κ -Cl under H_b ($> H_b^{\text{SRT}}$), $SS^{\text{Cl}}(H_b > H_b^{\text{SRT}})$. In all cases, local moments at A1–B2 sublattices are shown in red. Green arrows, M_F^{A} and M_F^{B} , indicate ferromagnetic components of sublattice magnetizations in layers A and B, respectively, which are perpendicular to the DM vectors D_{A} and D_{B} , shown by black arrows. In the cases of (b) and (d), M_F^{A} and M_F^{B} are not exactly perpendicular to the DM vectors, owing to the Zeeman effect.

field further, presuming that d8- κ -Br has $SS^{\text{Br}}(0)$, to confirm the validity of our scenario.

C. Field-induced spin reorientation phenomena in d8- κ -Br

We also claimed [1] that h8- κ -Cl undergoes unusual spin reorientation transition under H_b . This is corresponding to the magnetization jump of $M(H_b)$ at approximately 4 kOe, as observed in the inset of Fig. 6(b). Although this magnetization jump has been regarded as a conventional spin flop transition for a long time [3,11,12], we revised the interpretation of this phenomenon. We concluded that the spins in layer B suddenly reverse at the critical value of H_b . In this paper, this phenomenon and the critical field are referred to as spin-reverse transition (SRT) and H_b^{SRT} , respectively. In addition, the spin structure under H_i is referred to as $SS^{\text{Cl}}(H_i)$ with

$i = a, b$, and c . Further, we refer to the spin structure under H_b higher than H_b^{SRT} as $\text{SS}^{\text{Cl}}(H_b > H_b^{\text{SRT}})$. Figure 8 shows $\text{SS}^{\text{Cl}}(H_b > H_b^{\text{SRT}})$ as well as $\text{SS}^{\text{Cl}}(0)$ viewed from the b -axis direction. In the figure, \mathbf{M}_F indicates the four sublattice magnetizations corresponding to the net canting moment. A schematic of them viewed from the c -axis direction is also shown in Figs. 9(c) and 9(d) together with the DM vectors and the two sublattice magnetizations corresponding to the local canting moments, \mathbf{M}_F^{A} and \mathbf{M}_F^{B} . As shown in the figures, the difference between $\text{SS}^{\text{Cl}}(0)$ and $\text{SS}^{\text{Cl}}(H_b > H_b^{\text{SRT}})$ manifests itself only in layer B: the spins as well as the local canting moment in layer B rotate by 180° around \mathbf{D}_B .

Figure 9(a) shows the proposed ZF spin structure of d8- κ -Br, $\text{SS}^{\text{Br}}(0)$. Interestingly, this spin structure is essentially the same as $\text{SS}^{\text{Cl}}(H_b > H_b^{\text{SRT}})$. The response of $\text{SS}^{\text{Br}}(0)$ against the magnetic field can be easily predicted using the analogy of h8- κ -Cl. In the case of d8- κ -Br, the application of H_a is expected to induce a transition similar to SRT of h8- κ -Cl. This field-induced phenomenon in d8- κ -Br is also referred to as SRT and the critical value of H_a is referred to as H_a^{SRT} . Figure 9(b) shows the proposed spin structure under H_a higher than H_a^{SRT} , referred to as $\text{SS}^{\text{Br}}(H_a > H_a^{\text{SRT}})$. In this process, the direction of the net canting moment changes from the b axis to the a axis, and as in the case of SRT in h8- κ -Cl the spins and the local canting moment in layer B rotate by 180° around \mathbf{D}_B . Moreover, $\text{SS}^{\text{Br}}(H_a > H_a^{\text{SRT}})$ is essentially the same as $\text{SS}^{\text{Cl}}(0)$. Ultimately, it has been suggested that only two types of spin structures are realized, depending on the material (d8- κ -Br or h8- κ -Cl) and the magnetic field (ZF or H_a or H_b). A comparison between this prediction and the observation enables us to claim that the SRT predicted for d8- κ -Br will correspond to the steplike behavior under H_a in the inset of Fig. 6(a).

An application of H_a to h8- κ -Cl allows the canting moment to be enhanced gradually with the basic spin structure unchanged, which can be easily understood by observing Figs. 8(c) and 9(c). This is the simplest spin reorientation, and reflecting this fact the magnetization under H_a exhibits a simple linear dependence on H_a down to ZF, as observed in Fig. 6(b). Similarly, d8- κ -Br under H_b is expected to exhibit such a simple spin reorientation. In fact, the magnetization under H_b of d8- κ -Br exhibits such a behavior before the magnetization is enhanced by pinned vortices of the minor SC phase, as observed in Fig. 6(a). As explained in Sec. III D, it appears as if the behaviors of $M(H_a)$ and $M(H_b)$ in h8- κ -Cl are replaced by the reverse combination in d8- κ -Br. Assigning a spin structure to the two materials proves the reversal of the magnetization behaviors between the two materials.

We also claimed that h8- κ -Cl exhibits another intriguing spin reorientation under H_c . Hereafter, the spin structures of h8- κ -Cl and d8- κ -Br under H_c are referred to as $\text{SS}^{\text{Cl}}(H_c)$ and $\text{SS}^{\text{Br}}(H_c)$, respectively. The local canting moment in layer A of h8- κ -Cl is roughly directed to the $a + b$ direction at ZF, as observed in Fig. 10(b). The application of H_c allows this canting moment to be directed to the c axis. Simultaneously, the local moment at the A1 (A2) sublattice changes its orientation from the $-c$ ($+c$) to the $a + b$ ($-a - b$) direction. Moreover, in layer B, a similar spin reorientation is expected to occur. When the local moments are viewed from the starting

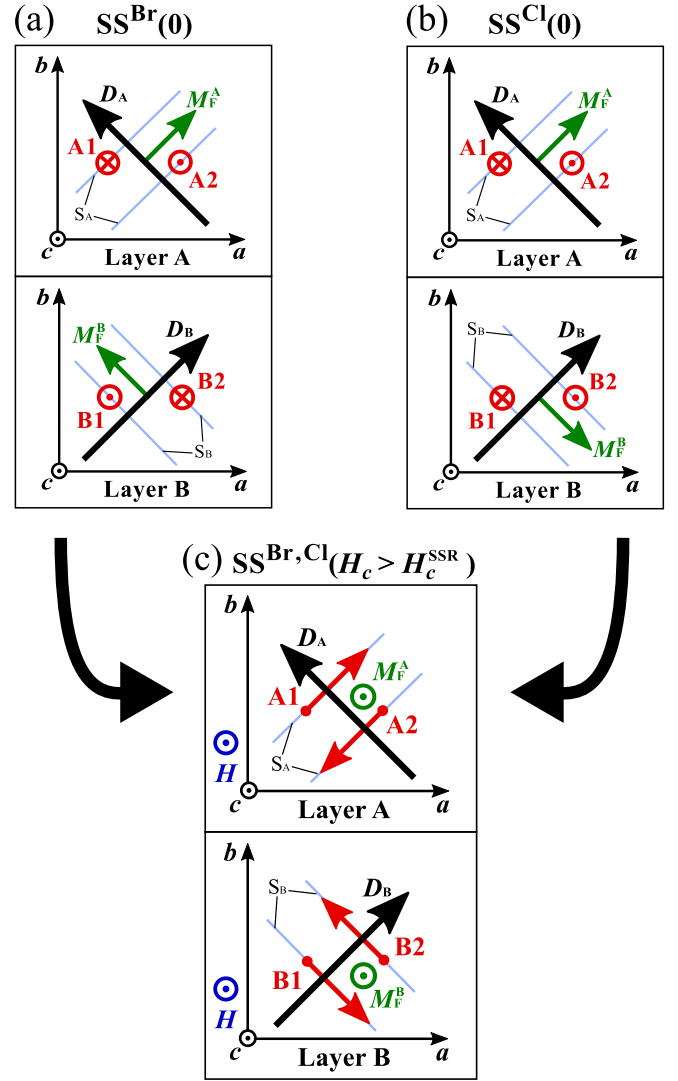


FIG. 10. ZF spin structures of d8- κ -Br, $\text{SS}^{\text{Br}}(0)$ (a) and h8- κ -Cl, $\text{SS}^{\text{Cl}}(0)$ (b), which are the same as those in Figs. 9(a) and 9(c), respectively. Blue lines represent S_A and S_B , which are explained in Fig. 7 as the planes perpendicular to the DM vectors, \mathbf{D}_A and \mathbf{D}_B , respectively. (c) Spin structure under H_c larger than H_c^{SSR} , which is the field at which the local canting moments corresponding to \mathbf{M}_F^{A} and \mathbf{M}_F^{B} become parallel to the magnetic field (c axis). We refer to the spin structures of d8- κ -Br and h8- κ -Cl under $H_c > H_c^{\text{SSR}}$ as $\text{SS}^{\text{Br}}(H_c > H_c^{\text{SSR}})$ and $\text{SS}^{\text{Cl}}(H_c > H_c^{\text{SSR}})$, respectively. In our model, the local moments always lie in S_A and S_B during the entire process.

point of the DM vectors, the local moments as well as the local canting moments in both layers rotate anticlockwise by 90° with increasing magnetic field up to a certain level. Following this, the spin rotation stops and only the increase in canting moment is maintained. This is also an intriguing spin reorientation phenomenon. We define the magnetic field at which the canting moment becomes parallel to the field direction as H_c^{SSR} , in which SSR denotes the saturation of the spin rotation. We also refer to the spin structure under magnetic fields below and above H_c^{SSR} as $\text{SS}^{\text{Cl}}(H_c < H_c^{\text{SSR}})$ and $\text{SS}^{\text{Cl}}(H_c > H_c^{\text{SSR}})$, respectively.

Also, in d8- κ -Br, a phenomenon similar to the above-mentioned spin reorientation is expected to occur. As the spin structure in layer A of d8- κ -Br is the same as that of h8- κ -Cl, the responses in layer A against H_c will be the same. In contrast, the local moments as well as the local canting moments in layer B of d8- κ -Br will rotate reversely with increasing magnetic field. Following this, a similar saturation behavior of the spin rotation will occur. Finally, the spin structure of the two materials becomes identical under high fields, as demonstrated in Fig. 10. We also refer to the magnetic field at which the canting moment becomes parallel to the field direction as H_c^{SSR} for d8- κ -Br. The spin structures under and above H_c^{SSR} are referred to as $\text{SS}^{\text{Br}}(H_c < H_c^{\text{SSR}})$ and $\text{SS}^{\text{Br}}(H_c > H_c^{\text{SSR}})$, respectively. These abbreviations can be used to express $\text{SS}^{\text{Br}}(H_c > H_c^{\text{SSR}}) \equiv \text{SS}^{\text{Cl}}(H_c > H_c^{\text{SSR}})$. Although $\text{SS}^{\text{Br}}(H_c < H_c^{\text{SSR}})$ is different from $\text{SS}^{\text{Cl}}(H_c < H_c^{\text{SSR}})$, there is almost no difference in the response of the c -axis component of the local canting moment against H_c among all spin pairs in the four layers (layers A and B in the two materials). This is the reason why the magnetization behaviors of the two materials under H_c are qualitatively similar to each other as observed in Fig. 6.

In this way, the magnetization behaviors of d8- κ -Br under magnetic fields parallel to the three crystallographic axes are qualitatively understood as consequences of the proposed spin reorientations, similar but meaningfully different phenomena of which can be found in the spin reorientations proposed for h8- κ -Cl. The reversal situation of $M(H_a)$ and $M(H_b)$ between the two materials as well as the common behavior of $M(H_c)$ can also be understood by presuming two different ZF spin structures. We also highlight that high-field spin structures proposed for the two materials are the same, which is consistent with results of previous studies. Thus, the interpretations of the magnetization processes support the validity of the proposed ZF spin structure of d8- κ -Br.

D. Quantitative analyses

Through the above discussion, an overall picture of the magnetism of d8- κ -Br, such as the ZF magnetic structure and the field-induced spin reorientations, can be obtained. In this section, to evaluate the strength of the interaction between spins, we analyze the magnetization on the basis of the classical spin model. For a quantitative analysis of the magnetization of d8- κ -Br, we must carefully investigate the contribution of the minor SC phase. However, as discussed in Sec. III C, we only have to focus on the underestimation of the magnetization of the AFI phase.

First, we attempt to estimate the strength of the interlayer interaction in d8- κ -Br, using the $M(H_a)$ data near SRT. The energy of the interlayer interaction is expressed as

$$E_{\perp} = 2A_{\perp}(\mathbf{M}_{A1} \cdot \mathbf{M}_{B1} + \mathbf{M}_{A2} \cdot \mathbf{M}_{B2}), \quad (3)$$

where A_{\perp} is an interlayer interaction parameter ($A_{\perp} > 0$ in d8- κ -Br). Two of the proposed spin structures, $\text{SS}^{\text{Br}}(0)$ and $\text{SS}^{\text{Br}}(H_a > H_a^{\text{SRT}})$, before and after SRT are shown in Figs. 9(a) and 9(b), respectively. The spin structure immediately before SRT is essentially the same as $\text{SS}^{\text{Br}}(0)$ except for the slight enhancement of the a -axis component of the local canting moment. As observed in the figures, the difference

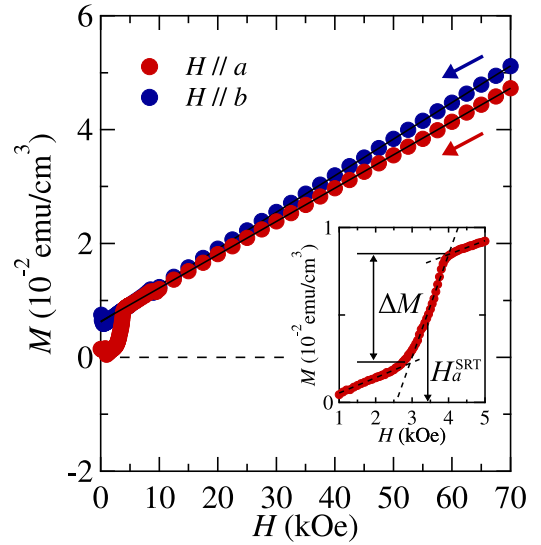


FIG. 11. Isothermal magnetizations of d8- κ -Br, $M(H_a)$ and $M(H_b)$, which are the same as those in Fig. 6(a). The solid lines are the lines used to fit Eq. (5). The inset shows the definitions of magnetization jump, ΔM , and the critical field of the spin-reverse transition, H_a^{SRT} .

between the two types of structures is only a rotation of half of the spin pairs (B1 and B2) by 180° . Therefore, the difference between the Zeeman energy immediately after and immediately before the SRT almost purely reflects the energy difference between the interlayer FM and AF arrangements, as discussed in the SRT of h8- κ -Cl [1]. Accordingly, we obtain [1] the relation

$$2|A_{\perp}|(2M_0)^2 \sim \Delta M(H_a = H_a^{\text{SRT}})H_a^{\text{SRT}}, \quad (4)$$

where M_0 and $\Delta M(H_a = H_a^{\text{SRT}})$ are the magnitude of the sublattice magnetization and the magnetization difference at SRT, respectively. As demonstrated in the inset of Fig. 11, we evaluated the values of H_a^{SRT} and $\Delta M(H_a = H_a^{\text{SRT}})$. These values as well as the local moment of $0.26 \mu_B$ estimated by ^{13}C -NMR [25] enabled us to obtain the value of A_{\perp} . Using this value, we converted to the microscopic interlayer interaction, J_{\perp}^* , as 3.4×10^{-4} meV. In our previous paper [1], we suggested the possibility of AF exchange interaction between diagonal sublattices (for example, A1 and B2 sublattices) for the origin of the interlayer ferromagnetic arrangement of h8- κ -Cl. In this sense, J_{\perp}^* may be written as $J_{\perp}^{1\text{st}} - 4J_{\perp}^{2\text{nd}}$, where $J_{\perp}^{1\text{st}}$ and $J_{\perp}^{2\text{nd}}$ are the interlayer interaction between the nearest-neighbor sublattices and that between the diagonal sublattices, respectively. We also estimated the value of J_{\perp}^* from $M^*(H_a)$, which was corrected by considering the inclusion of 15% of the paramagnetic component, as 4.0×10^{-4} meV. These values are listed in Table I. We have already applied [1] the same analytical method to the SRT of h8- κ -Cl and obtained the value of J_{\perp}^* as -2.31×10^{-4} meV, as listed in the table. Although the signs of J_{\perp}^* of the two materials are, of course, opposite to each other, they are common in that both the absolute values are small in magnitude. In contrast, the interlayer AF arrangement in d8- κ -Br is naturally understood by considering the effect of the AF exchange interaction between

TABLE I. Microscopic parameters of d8- κ -Br obtained from the analyses of the data of $M(H_a)$ and $M(H_b)$ and those of h8- κ -Cl in our previous paper [1]. J_{\parallel} , $(D_{12})_a$, and $(D_{12})_b$ are strengths of intralayer exchange interaction and a and b components of microscopic DM interaction, respectively, obtained from the fitting results of $M(H_a)$ and $M(H_b)$ by Eq. (5). J_{\perp}^* is a strength of converted interlayer interaction, which may be able to be defined as $J_{\perp}^{1st} - 4J_{\perp}^{2nd}$. As for the definitions, see text. In the case of d8- κ -Br, the value was obtained from the data of $M(H_a)$ by Eq. (4). $M^*(H_a)$ and $M^*(H_b)$ denote corrected magnetizations by taking 15% of the paramagnetic component into consideration.

	J_{\parallel} (meV)	J_{\perp}^* (10^{-4} meV)	$(D_{12})_a$ (meV)	$(D_{12})_b$ (meV)
d8- κ -Br				
$M(H_a)$	55.7 ± 0.1	3.4 ± 0.2		0.241 ± 0.002
$M^*(H_a)$	47.4 ± 0.1	4.0 ± 0.2		0.241 ± 0.002
$M(H_b)$	51.0 ± 0.1		0.223 ± 0.001	
$M^*(H_b)$	43.3 ± 0.1		0.223 ± 0.001	
h8- κ -Cl				
$M(H_a)$	56.9 ± 0.1			0.277 ± 0.001
$M(H_b)$	50.6 ± 0.1	-2.31 ± 0.04	0.246 ± 0.001	

neighboring sublattices (for example, A1 and B1 sublattices). However, in such a situation, the magnitude of the interlayer interaction is typically extremely small. Therefore, J_{\perp}^{1st} and $4J_{\perp}^{2nd}$ may compete with each other in the two materials. In addition to this situation, the dipole interaction may play an important role in the interlayer interaction in h8- κ -Cl.

As the interlayer interaction was confirmed to be extremely weak, we can adopt a simple model while only taking account of the intralayer exchange and DM interactions for the analysis of the high-field magnetization data of d8- κ -Br. Smith *et al.* used the following formula for the analysis of the high-field magnetization data of h8- κ -Cl [11]:

$$M(H_i) = \frac{M_0 C_i + H_i}{A_{\parallel}}, \quad (5)$$

where $i = a, b$, and c and $C_a = D_b$, $C_b = D_a$, and $C_c = \sqrt{D_a^2 + D_b^2}$. This formula is also applicable to d8- κ -Br. We fitted the data of $M(H_a)$ and $M(H_b)$ above 30 kOe by linear functions, as shown in Fig. 11. Using the fitted data, we estimated the intralayer exchange parameter, A_{\parallel} , and the a and b components of the DM interaction, D_a and D_b . These values were then transformed into values of the microscopic parameters such as intralayer exchange interaction, J_{\parallel} , and a and b components of the microscopic DM interaction, $(D_{12})_a$ and $(D_{12})_b$, and are listed in Table I together with those obtained in h8- κ -Cl in our previous paper [1]. As for d8- κ -Br, the values obtained after correcting the magnetization considering the underestimation mentioned above are also listed.

Except for the interlayer interaction, there is almost no difference in the listed values of the two materials. In particular, it may be incomprehensible that the absolute value of the interlayer interaction of d8- κ -Br ($T_N = 11.8$ K) is roughly two times larger than that of h8- κ -Cl ($T_N = 22.8$ K) as it is generally known that T_N strongly depends on the strength of

the interlayer interaction in quasi-two-dimensional magnets. By a process of elimination, this appreciable difference in T_N may originate from the factor 2 difference of the value of the local moment ($0.4\text{--}0.5 \mu_B$ for h8- κ -Cl [3] and $0.26 \mu_B$ for d8- κ -Br [25]). As another possibility, the so-called anisotropic energy (hereafter referred to as K_c) that plays a role of forcing the spins to point toward $+c$ or $-c$ directions might contribute the magnetic ordering in the present systems, as discussed in recent work [45]. Indeed this effect in h8- κ -Cl is estimated to be much larger than that in d8- κ -Br, as mentioned in the next section. In contrast, common characteristic properties such as the near absence of in-plane anisotropy in J_{\parallel} and a proximity of the values of $(D_{12})_a$ and $(D_{12})_b$ are consistent with the results obtained until now. For example, Smith *et al.* claimed that $(D_{12})_a \simeq (D_{12})_b$ from ^{13}C -NMR measurements on h8- κ -Cl [15], as mentioned above. In this way, the magnetic properties of d8- κ -Br are found to be very similar to those of h8- κ -Cl, except for the interlayer interaction and the values of T_N and K_c .

E. Simulation of M and comparison with the experimental data

In this section, we attempt to reproduce the characteristic behaviors in $M(H_a)$ and $M(H_c)$ of d8- κ -Br by carrying out numerical simulations based on the classical spin model. The total energy of the spin system of d8- κ -Br, E^{Br} , under the magnetic field, \mathbf{H} , can be written by

$$E^{\text{Br}} = E_{\text{AF}} + E_{\text{DM}} + E_{\perp} - \mathbf{H} \cdot (\mathbf{M}_{\text{A1}} + \mathbf{M}_{\text{A2}} + \mathbf{M}_{\text{B1}} + \mathbf{M}_{\text{B2}}). \quad (6)$$

The aim in this simulation study was to use the parameters obtained by the analyses of $M(H_a)$ and $M(H_c)$ as little as possible. Accordingly, we used the parameters obtained by the analysis of $M(H_b)$: the macroscopic values corresponding to 51.0 and 0.223 meV are used as fixed values of A_{\parallel} and D_a , respectively. We assume that $D_a = D_b$, as in the case of h8- κ -Cl; that the intralayer exchange interaction is isotropic; and that a dimer has a local moment of $0.26 \mu_B$. In addition, we exceptionally use the value of A_{\perp} (corresponding to 3.4×10^{-4} meV) obtained by Eq. (4). By using these values, we simulated the expected $M(H_a)$ and $M(H_c)$ by determining the minimum values of Eq. (6) at various magnetic fields. Details of this simulation are provided in our previous paper [1], where essentially the same simulation method was applied to $M(H_b)$ and $M(H_c)$ in h8- κ -Cl. Figure 12 compares the experimental and simulation results. In the simulation results, SRT and SSR are clearly observed as a magnetization jump at ≈ 3 kOe [Fig. 12(a)] and a kink structure at ≈ 2 kOe [Fig. 12(b)], respectively. Although the experimental data exhibit more gradual anomalies at almost the same magnetic fields for both cases, the simulation results qualitatively well reproduce the observations. The smoothing at these anomalies will be caused by the disorder effect on the spin system, which is inherent for d8- κ -Br. Indeed, the experimental data of $M(H_b)$ and $M(H_c)$ in h8- κ -Cl, which has a less disordered spin system, exhibited a sharp magnetization jump and a clear kink structure, similar to the simulation data.

In our model, we neglected the anisotropic energy, K_c . Whereas SRT is irrelevant to K_c , the field of SSR depends on the K_c as well as J_{\perp}^* . The good coincidence of the SSR field

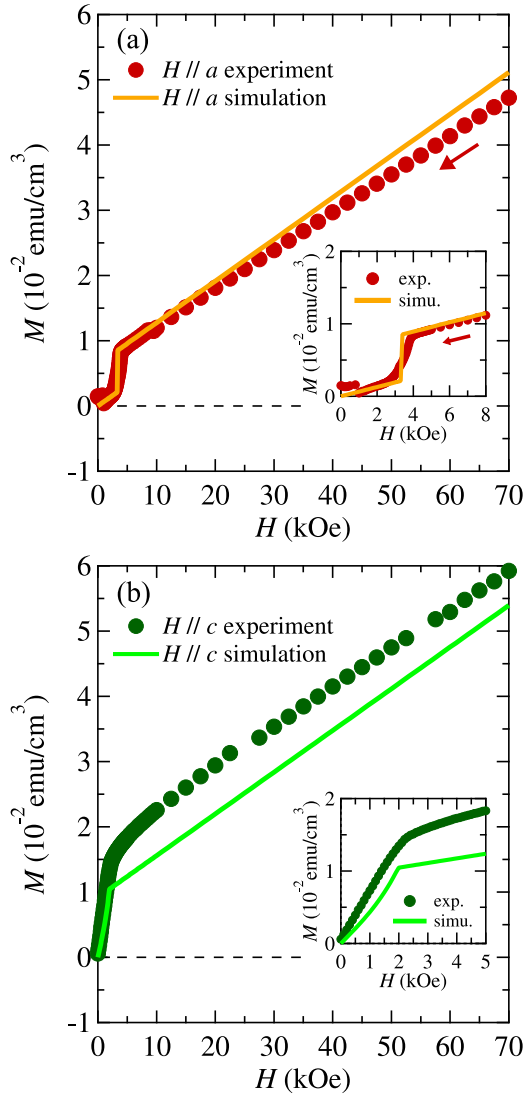


FIG. 12. Comparison between experimental and simulation results of $M(H_a)$ (a) and $M(H_c)$ (b) of $d8\text{-}\kappa\text{-Br}$. Insets: Expansions of them in the low-field region.

between simulated and measured magnetizations strongly suggests that the K_c is much smaller than J_{\perp}^* in $d8\text{-}\kappa\text{-Br}$. On the other hand, a simulated value of the field of SSR in $h8\text{-}\kappa\text{-Cl}$ is roughly a half of the measured SSR field [1]. This fact suggests that the K_c may contribute the magnetization process of $h8\text{-}\kappa\text{-Cl}$ under c -axis magnetic field. We assumed the K_c of which the magnitude is the same as the value of J_{\perp}^* and reperformed the simulation of the c -axis magnetization of $h8\text{-}\kappa\text{-Cl}$. As a result, we confirmed that, at least, the simulated and measured values of the SSR field coincide with each other. This result may be consistent with previous study, which suggested the K_c of which the magnitude is the same as J_{\perp}^* [46].

As a conclusion to this section, the agreement between the simulation and experimental results not only for $d8\text{-}\kappa\text{-Br}$ but also for $h8\text{-}\kappa\text{-Cl}$ strongly supports the validity of our scenario regarding ZF spin structures and spin reorientations in the two materials.

F. Symmetry analysis of the magnetically ordered phase based on crystal symmetry

Lastly, we verify our scenario from a different perspective. The space group of the crystal of $d8\text{-}\kappa\text{-Br}$ as well as $h8\text{-}\kappa\text{-Cl}$ is $Pnma$ [2]. We can choose four symmetry operations as the selected generators: a translational symmetry operation (\mathcal{R}) along the unit vectors, an inversion symmetry operation (\mathcal{I}) at the center of the dimer of BEDT-TTF, a glide symmetry operation (\mathcal{G}) at $(x, y, 1/4)$ planes [dashed lines in Fig. 1(b)], and a mirror symmetry operation (\mathcal{M}) at the anion plane. As with breaking the time-reversal symmetry (\mathcal{T}) in the magnetically ordered state, some of these symmetries will be broken with respect to pseudovectors. However, the former two symmetries (\mathcal{R} and \mathcal{I}) will not be broken in the ordered state of the present system. If these symmetries were broken, magnetic properties that are more complicated than the ones observed will be realized. For example, the local moment was known to be uniform on the dimer [25,47], which indicates that the symmetry \mathcal{I} is maintained in the ordered state (although multiple operators, \mathcal{RT} and \mathcal{IT} , may be possible from the viewpoint of magnetic symmetry, they can be excluded in the present materials exhibiting ferromagnetism [48]). Therefore, we only focus on \mathcal{G} and \mathcal{M} . As with breaking \mathcal{T} , there is the possibility of breaking some of \mathcal{G} and \mathcal{M} as well as multiple operators, \mathcal{GT} and \mathcal{MT} . However, \mathcal{G} (\mathcal{M}) is mutually exclusive with \mathcal{GT} (\mathcal{MT}). Therefore, we can select four of the most symmetric states that maintain the combinations of the symmetries, \mathcal{GT} and \mathcal{MT} , \mathcal{GT} and \mathcal{M} , \mathcal{G} and \mathcal{MT} , as well as \mathcal{G} and \mathcal{M} .

Candidates of the spin structures with the highest symmetry are referred to as SS1–SS4, as listed in Table II. Four pairs of the symmetry operators in Table II allow us to fix possible orientations of the local moments at A1–B2 sites. The summation of the local moments, $\mathbf{m}_{\text{total}}$, exhibits an intriguing variation. This, of course, represents the direction of the ferromagnetism. All the results described above suggest that SS1 and SS2 correspond to $SS^{\text{Cl}}(0)$ and $SS^{\text{Br}}(0)$, respectively. The orientations of each local moment in SS1 and SS2 also agree with our assigned ZF spin structures of $h8\text{-}\kappa\text{-Cl}$ and $d8\text{-}\kappa\text{-Br}$, respectively. Therefore, $SS^{\text{Cl}}(0)$ and $SS^{\text{Br}}(0)$ are two of the structures that should be realized from a theoretical viewpoint.

It is also interesting that SS3 coincides with $SS^{\text{Br}}(H_c > H_c^{\text{SSR}}) [\equiv SS^{\text{Cl}}(H_c > H_c^{\text{SSR}})]$. This indicates that the application of H_c leads to forced ferromagnetism parallel to the c axis and consequently another highest symmetric spin structure is realized. In this sense, the kink structures at SSR in the two materials are phase transitions from a lower-symmetry state to a higher-symmetry one [49]. Indeed, the kink structures in the experimental data in $h8\text{-}\kappa\text{-Cl}$ as well as the simulation data in the two materials are very sharp, indicating that they are second-order phase transitions. The proposed field-induced spin structures, $SS^{\text{Br}}(H_a > H_a^{\text{SRT}})$ and $SS^{\text{Cl}}(H_b > H_b^{\text{SRT}})$, also agree with SS1 and SS2, respectively. Therefore, the SRTs of the two materials appear to be phase transitions to the highest-symmetry states. As for the rest of the spin structures, SS4, the zero value of the total local moment does not match the present two weak ferromagnets. In addition, this property is also impossible to be induced by applying a magnetic field.

TABLE II. Candidates of spin structures, referred to as SS1–SS4, taking account of glide symmetry (\mathcal{G}), mirror symmetry (\mathcal{M}), and time-reversal symmetry (\mathcal{T}). \mathbf{m}_{A1} – \mathbf{m}_{B2} are local moments at A1–B2 sites, respectively, and $\mathbf{m}_{\text{total}}$ is the summation of the local moments.

	Symmetry	\mathbf{m}_{A1}	\mathbf{m}_{A2}	\mathbf{m}_{B1}	\mathbf{m}_{B2}	$\mathbf{m}_{\text{total}}$
SS1	$\mathcal{GT}, \mathcal{MT}$	(m_a, m_b, m_c)	$(m_a, m_b, -m_c)$	$(m_a, -m_b, m_c)$	$(m_a, -m_b, -m_c)$	$(4m_a, 0, 0)$
SS2	$\mathcal{GT}, \mathcal{M}$	(m_a, m_b, m_c)	$(m_a, m_b, -m_c)$	$(-m_a, m_b, -m_c)$	$(-m_a, m_b, m_c)$	$(0, 4m_b, 0)$
SS3	$\mathcal{G}, \mathcal{MT}$	(m_a, m_b, m_c)	$(-m_a, -m_b, m_c)$	$(m_a, -m_b, m_c)$	$(-m_a, m_b, m_c)$	$(0, 0, 4m_c)$
SS4	\mathcal{G}, \mathcal{M}	(m_a, m_b, m_c)	$(-m_a, -m_b, m_c)$	$(-m_a, m_b, -m_c)$	$(m_a, -m_b, -m_c)$	$(0, 0, 0)$

Eventually, three of the highest-symmetry spin states manifest themselves in h8- κ -Cl and d8- κ -Br.

To conclude, our assigned spin structures of h8- κ -Cl and d8- κ -Br under zero and high magnetic fields are all preferable from the viewpoint of magnetic symmetry. Our claim regarding ZF spin structures and spin reorientations in the two materials has been further supported.

V. CONCLUSION

We elucidated static magnetism of the canted antiferromagnet, κ -(d8-BEDT-TTF)₂Cu[N(CN)₂]Br, under zero, low, and high magnetic fields by investigating isothermal magnetizations while suppressing the contribution of the minor superconducting phase as much as possible. Consequently, we succeeded in assigning a zero-field spin structure, which was surprisingly different from that of κ -(BEDT-TTF)₂Cu[N(CN)₂]Cl. Our spin model enabled us to conclude that this difference is caused by the difference in the sign of the interlayer interaction between the two materials. The difference in the pattern of the field-induced spin reorientations between the two materials is interpreted by our spin model

and is also reproduced in numerical simulations. Finally, the magnetic symmetry analysis supports the validity of our assigned spin structure of d8- κ -Br as well as h8- κ -Cl under zero and high magnetic fields. It has been revealed that three of the most symmetric spin structures manifest themselves, depending on the material and the orientation and intensity of the magnetic field. Although some of our assertions should be confirmed by microscopic proof in the future, we highlight that our scenario can only be constructed by analyzing the macroscopic phenomena originating from the tiny canting of the spins (approximately 0.2° at a zero magnetic field), which is not detectable at the microscopic probes. The present paper suggests that a hidden phase boundary should exist within the AFI phase in the popular pressure-temperature phase diagram of the κ -type organic system.

ACKNOWLEDGMENTS

This work was partially supported by Japan Society for the Promotion of Science KAKENHI Grant No. 16K05433. We thank K. Miyagawa at University of Tokyo for fruitful discussions.

-
- [1] R. Ishikawa, H. Tsunakawa, K. Oinuma, S. Michimura, H. Taniguchi, K. Satoh, Y. Ishii, and H. Okamoto, *J. Phys. Soc. Jpn.* **87**, 064701 (2018).
- [2] U. Geiser, A. J. Schultz, H. H. Wang, D. M. Watkins, D. L. Stupka, and J. M. Williams, *Physica C* **174**, 475 (1991).
- [3] K. Miyagawa, A. Kawamoto, Y. Nakazawa, and K. Kanoda, *Phys. Rev. Lett.* **75**, 1174 (1995).
- [4] H. Kino and H. Fukuyama, *J. Phys. Soc. Jpn.* **64**, 2726 (1995).
- [5] K. Kanoda, *Hyperfine Interact.* **104**, 235 (1997).
- [6] K. Kanoda, *J. Phys. Soc. Jpn.* **75**, 051007 (2006).
- [7] K. Kanoda, *Physica C* **282–287**, 299 (1997).
- [8] M. Ito, T. Uehara, H. Taniguchi, K. Satoh, Y. Ishii, and I. Watanabe, *J. Phys. Soc. Jpn.* **84**, 053703 (2015).
- [9] I. Dzyaloshinsky, *J. Phys. Chem. Solids* **4**, 241 (1958).
- [10] T. Moriya, *Phys. Rev.* **120**, 91 (1960).
- [11] D. F. Smith, S. M. De Soto, C. P. Slichter, J. A. Schlueter, A. M. Kini, and R. G. Daugherty, *Phys. Rev. B* **68**, 024512 (2003).
- [12] S. M. Winter, K. Riedl, and R. Valentí, *Phys. Rev. B* **95**, 060404(R) (2017).
- [13] U. Welp, S. Fleshler, W. K. Kwok, G. W. Crabtree, K. D. Carlson, H. H. Wang, U. Geiser, J. M. Williams, and V. M. Hitsman, *Phys. Rev. Lett.* **69**, 840 (1992).
- [14] F. Kagawa, Y. Kurosaki, K. Miyagawa, and K. Kanoda, *Phys. Rev. B* **78**, 184402 (2008).
- [15] D. F. Smith, C. P. Slichter, J. A. Schlueter, A. M. Kini, and R. G. Daugherty, *Phys. Rev. Lett.* **93**, 167002 (2004).
- [16] S. Lefebvre, P. Wzietek, S. Brown, C. Bourbonnais, D. Jérôme, C. Mézière, M. Fourmigue, and P. Batail, *Phys. Rev. Lett.* **85**, 5420 (2000).
- [17] A. M. Kini, U. Geiser, H. H. Wang, K. D. Carlson, J. M. Williams, W. K. Kwok, K. G. Vandervoort, J. E. Thompson, D. L. Stupka, D. Jung, and M.-H. Whangbo, *Inorg. Chem.* **29**, 2555 (1990).
- [18] A. Kawamoto, K. Miyagawa, and K. Kanoda, *Phys. Rev. B* **55**, 14140 (1997).
- [19] A. Kawamoto, H. Taniguchi, and K. Kanoda, *J. Am. Chem. Soc.* **120**, 10984 (1998).
- [20] M. de Souza, A. Brühl, C. Strack, B. Wolf, D. Schweitzer, and M. Lang, *Phys. Rev. Lett.* **99**, 037003 (2007).
- [21] H. Taniguchi, A. Kawamoto, Y. Nakazawa, and K. Kanoda, *Synth. Met.* **103**, 2250 (1999).
- [22] H. Taniguchi, A. Kawamoto, and K. Kanoda, *Physica B* **284–288**, 519 (2000).
- [23] Y. Nakazawa, H. Taniguchi, A. Kawamoto, and K. Kanoda, *Phys. Rev. B* **61**, R16295 (2000).
- [24] H. Ito, T. Ishiguro, T. Kondo, and G. Saito, *J. Phys. Soc. Jpn.* **69**, 290 (2000).

- [25] K. Miyagawa, A. Kawamoto, and K. Kanoda, *Phys. Rev. Lett.* **89**, 017003 (2002).
- [26] M. Tokumoto, N. Kinoshita, Y. Tanaka, and H. Anzai, *Mater. Res. Soc. Symp. Proc.* **488**, 903 (1998).
- [27] H. Taniguchi, A. Kawamoto, and K. Kanoda, *Phys. Rev. B* **59**, 8424 (1999).
- [28] T. Nishi, S. Kimura, T. Takahashi, T. Ito, H. J. Im, Y. S. Kwon, K. Miyagawa, H. Taniguchi, A. Kawamoto, and K. Kanoda, *Solid State Commun.* **134**, 189 (2005).
- [29] T. Sasaki, N. Yoneyama, A. Suzuki, N. Kobayashi, Y. Ikemoto, and H. Kimura, *J. Phys. Soc. Jpn.* **74**, 2351 (2005).
- [30] T. Sasaki, N. Yoneyama, N. Kobayashi, Y. Ikemoto, and H. Kimura, *Phys. Rev. Lett.* **92**, 227001 (2004).
- [31] T. Sasaki, I. Ito, N. Yoneyama, N. Kobayashi, N. Hanasaki, H. Tajima, T. Ito, and Y. Iwasa, *Phys. Rev. B* **69**, 064508 (2004).
- [32] H. Taniguchi, K. Kanoda, and A. Kawamoto, *Phys. Rev. B* **67**, 014510 (2003).
- [33] J. Müller, M. Lang, F. Steglich, J. A. Schlueter, A. M. Kini, and T. Sasaki, *Phys. Rev. B* **65**, 144521 (2002).
- [34] X. Su, F. Zuo, J. A. Schlueter, A. M. Kini, and J. M. Williams, *Phys. Rev. B* **58**, R2944 (1998).
- [35] H. Akutsu, K. Saito, and M. Sorai, *Phys. Rev. B* **61**, 4346 (2000).
- [36] T. Uehara, M. Ito, J. Angel, J. Shimada, N. Komakine, T. Tsuchiya, H. Taniguchi, K. Satoh, K. Triyana, Y. Ishii, and I. Watanabe, *J. Phys. Soc. Jpn.* **85**, 024710 (2016).
- [37] T. Ishiguro, K. Yamaji, and G. Saito, *Organic Superconductors*, 2nd ed. (Springer-Verlag, Berlin, 1997).
- [38] J. Angel, T. Uehara, J. Shimada, N. Komakine, T. Tsuchiya, H. Taniguchi, I. Watanabe, and K. Triyana, in *Advances of Science and Technology for Society: Proceedings of the 1st International Conference on Science and Technology 2015 (ICST-2015)*, edited by T. R. Nuringtyas, R. Roto, A. Widyaparaga, M. Mahardika, A. Kusumaadmaja, and N. Hadi, AIP Conf. Proc. No. 1755 (AIP, New York, 2016), p. 150011.
- [39] C. H. Mielke, N. Harrison, D. G. Rickel, A. H. Lacerda, R. M. Vestal, and L. K. Montgomery, *Phys. Rev. B* **56**, R4309 (1997).
- [40] H. Tsunakawa, R. Ishikawa, H. Taniguchi, K. Satoh, Y. Ishii, and I. Watanabe (unpublished).
- [41] F. Zuo, S. Khizroev, G. C. Alexandrakis, J. A. Schlueter, U. Geiser, and J. M. Williams, *Phys. Rev. B* **52**, R13126 (1995).
- [42] S. Khizroev, F. Zuo, G. C. Alexandrakis, J. A. Schlueter, U. Geiser, and J. M. Williams, *J. Appl. Phys.* **79**, 6586 (1996).
- [43] L. Fruchter, A. Aburto, and C. Pham-Phu, *Phys. Rev. B* **56**, R2936 (1997).
- [44] H. Taniguchi and K. Kanoda, *Synth. Met.* **103**, 1967 (1999).
- [45] Á. Antal, T. Fehér, B. Náfrádi, L. Forró, and A. Jánossy, *J. Phys. Soc. Jpn.* **84**, 124704 (2015).
- [46] Á. Antal, T. Fehér, A. Jánossy, E. Tátrai-Szekeres, and F. Fülöp, *Phys. Rev. Lett.* **102**, 086404 (2009).
- [47] A. Kawamoto, K. Miyagawa, Y. Nakazawa, and K. Kanoda, *Phys. Rev. B* **52**, 15522 (1995).
- [48] From the viewpoint of the symmetry analysis, it is possible that the two materials have magnetic order while possessing \mathcal{IT} (\mathcal{RT}) symmetry. In addition, the mixture of \mathcal{IT} (\mathcal{RT}) and \mathcal{I} (\mathcal{R}) symmetries, where some sites (some links of sites) possess \mathcal{IT} (\mathcal{RT}) symmetry and the other keep \mathcal{I} (\mathcal{R}) symmetry, could not be ruled out. However, the ferromagnetism should vanish when even one site (one link of the site) possessing \mathcal{IT} (\mathcal{RT}) symmetry exists in the ordered state, which is the reason why the \mathcal{IT} and \mathcal{RT} symmetries can be excluded in the present magnets.
- [49] Whereas $\text{SS}^{\text{Cl}}(0)$ possesses \mathcal{GT} and \mathcal{MT} symmetries, \mathcal{GT} symmetry breaks under c -axis magnetic field. On the other hand, whereas $\text{SS}^{\text{Br}}(0)$ possesses \mathcal{GT} and \mathcal{M} symmetries, both symmetries break in $d8\text{-}\kappa\text{-Br}$ under c -axis magnetic field. Therefore SSR in $h8\text{-}\kappa\text{-Cl}$ is a transition from a lower-symmetry (\mathcal{MT}) state to a higher-symmetry (\mathcal{G} and \mathcal{MT}) one and SSR in $d8\text{-}\kappa\text{-Br}$ is a transition from a lower-symmetry (no symmetry) state to a higher-symmetry (\mathcal{G} and \mathcal{MT}) one.